
Article:
Spaiardi, P., Giunta, R., Rispoli, G. et al. (2 more authors) (2025) Transient capacitance changes recorded from vestibular type I hair cells are produced by GK,L gating and do not involve neurotransmitter exocytosis. The Journal of Physiology. ISSN: 0022-3751

https://doi.org/10.1113/jp288645

The Journal of Physiology

Transient capacitance changes recorded from vestibular type I hair cells are produced by $G_{K,L}$ gating and do not involve neurotransmitter exocytosis

Paolo Spaiardi[1,2,3], Roberta Giunta[1], Giorgio Rispoli[4], Sergio Masetto[1] and Stuart L. Johnson[5,6]

[1]*Department of Brain and Behavioural Sciences, University of Pavia, Pavia, Italy*
[2]*Department of Biology and Biotechnology, University of Pavia, Pavia, Italy*
[3]*Department of Physics, INFN – Pavia Section, Pavia, Italy*
[4]*Department of Neuroscience and Rehabilitation, University of Ferrara, Ferrara, Italy*
[5]*School of Biosciences, University of Sheffield, Sheffield, UK*
[6]*Neuroscience Institute, University of Sheffield, Sheffield, UK*

Handling Editors: Nathan Schoppa & Tina Pangršič

The peer review history is available in the Supporting information section of this article (https://doi.org/10.1113/JP288645#support-information-section).

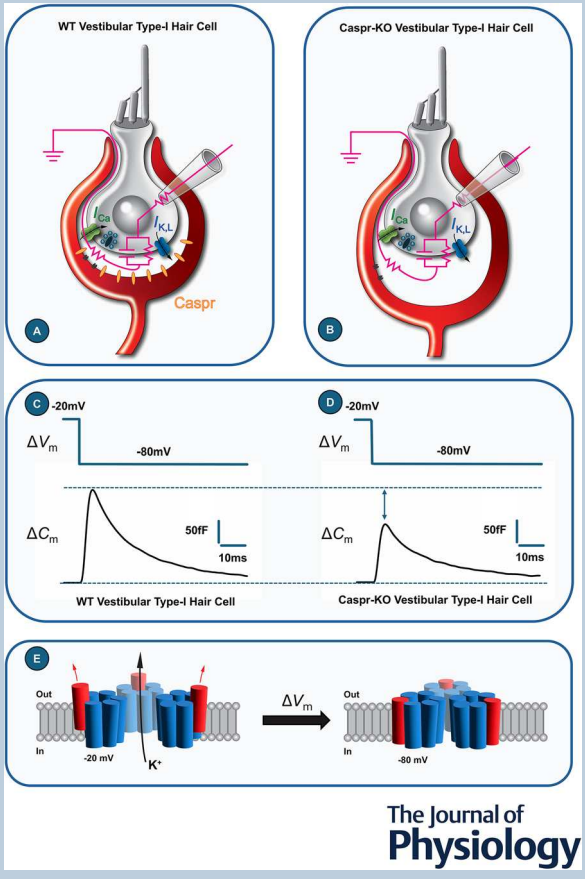

Abstract figure legend Schematic diagrams of mammalian wild type (WT) (A) and *Caspr*-KO (B) type-I vestibular hair cells showing localization of the Caspr protein (orange), the Ca^{2+} conductance (green) and the low-voltage-activated

S. Masetto and S. L. Johnson contributed equally to this work.

DOI: 10.1113/JP288645

K^+ conductance (blue). In WT cells, Caspr is localized at the calyceal membrane, where it is essential for maintaining the junctional contact between the hair cell basolateral membrane and the afferent neuron. In *Caspr*-KO cells (B), the absence of Caspr results in a significant increase in the gap between the hair cell and the afferent nerve terminal, leading to a decreased resistance within the calyceal synaptic cleft. Simplified electrical circuits are overlaid on the hair cell diagrams in pink.
Whole-cell patch-clamp recordings of changes in membrane capacitance (ΔC_m) reveal a large transient ΔC_m upon membrane hyperpolarization (C and D). The transient ΔC_m, which is Ca^{2+}-independent and unrelated to vesicle fusion during exocytosis, is considerably smaller in *Caspr*-KO type-I hair cells compared to WT. This finding suggests that the high resistance of the calyceal cleft in WT cells may amplify the ΔC_m transient.
The amplitude of the transient ΔC_m closely correlates with the level of activation of the low-voltage activated outward rectifying K^+ current ($I_{K,L}$) (through the blue channel in A and B). This relationship indicates that the transient ΔC_m likely originates from charge mobilization during the gating of K,L channels (cross-sectional illustration in E), rather than from vesicle fusion events.

Abstract Head movements are detected and signalled to primary sensory neurons by vestibular types I and II hair cells. Signal transmission involves glutamate exocytosis from hair cells, which is triggered by Ca^{2+} inflow through voltage-gated $Ca_V1.3$ Ca^{2+} channels. In a previous study on mice, we reported a Ca^{2+}-dependent exocytosis in both hair cell types, measured as a sustained change in cell membrane capacitance (ΔC_m) following cell depolarization, which was significantly smaller in type I than in type II hair cells. By contrast, only type I hair cells showed a large transient ΔC_m, which was still present in $Ca_V1.3^{-/-}$ mouse type I hair cells. Here we investigated the nature of this transient ΔC_m. We found that it was unaffected by 10 mM intracellular EGTA, which blocked most of the sustained exocytosis in these cells, demonstrating its insensitivity to intracellular Ca^{2+}. Moreover the amplitude of the transient ΔC_m correlated with the degree of activation of the low-voltage activated outward rectifying K^+ conductance, $G_{K,L}$, expressed by type I, but not type II hair cells. Finally the sign and kinetics of the transient ΔC_m changed based on voltage steps activating or deactivating $G_{K,L}$. These findings are consistent with the transient ΔC_m arising from the mobilization of charges during the gating of K,L channels, while excluding fast transient neurotransmitter exocytosis. Its large amplitude can be explained by the high resistance of the calyceal synaptic cleft since it was significantly reduced in $Caspr^{-/-}$ mice, which show a significantly larger synaptic cleft compared to wild type mice.

(Received 11 February 2025; accepted after revision 9 July 2025; first published online 26 August 2025)
Corresponding authors P. Spaiardi: Department of Brain and Behavioural Sciences, University of Pavia, Pavia, Italy. Email: paolo.spaiardi@unipv.it; S. L. Johnson: School of Biosciences, University of Sheffield, Sheffield, UK. Email: s.johnson@sheffield.ac.uk

Key points

- Vestibular type I and type II hair cells signal head movement to the central nervous system.
- Signal transmission from both hair cell types relies on Ca^{2+}-dependent glutamate exocytosis, measured here as a sustained change in cell membrane capacitance (ΔC_m). Type I hair cells exhibit also a large transient ΔC_m, whose nature has not been elucidated.
- In this study we found that the transient ΔC_m does not involve exocytosis, but it is generated by the gating of the low-voltage activated outward rectifying K^+ conductance, specifically expressed in type I hair cells.
- Transient ΔC_m analysis (also carried out in mice lacking the core protein of the septate-like junction) conclusively demonstrates that type I hair cells, like type II ones, do not elicit a transient release of neurotransmitter.
- Knowledge of the basic mechanisms of vestibular signalling is crucial in the study of pharmacological treatment for vestibular disorders and in the drug side effects targeted there.

Introduction

Vestibular organs of Amniotes are endowed with two types of sensory cells, called type I and type II hair cells. The most striking difference between type I and type II hair cells is their innervation. Although type II hair cells are contacted by several (10–20) small afferent and efferent nerve terminal boutons, type I hair cells are enclosed in a single giant afferent nerve terminal, called a calyx. The calyx synapse is a unique structure, characterized by both conventional quantal glutamatergic transmission (Bonsacquet et al., 2006; Matsubara et al., 1999; Sadeghi et al., 2014) and non-quantal afferent transmission (K^+ accumulation and ephaptic transmission; Contini et al., 2012, 2017, 2022, 2024; Govindaraju et al., 2023; Holt et al., 2007; Lim et al., 2011; Mukhopadhyay & Pangrsic, 2022; Songer & Eatock 2013; Yamashita & Omori, 1990). The membrane conductance of type I hair cells is dominated by $G_{K,L}$, a large K^+ conductance which involves the $K_V1.8$ subunit (Martin et al., 2024), and is functionally characterized by activating at unusually hyperpolarized membrane voltages (V_m, about −100 mV), being fully activated at around the cell resting V_m (−60 mV: Rennie & Correia 1994; Rüsch & Eatock 1996). $G_{K,L}$ is not present in type II hair cells, and the afferent transmission at the type II hair cell bouton synapse has only been reported to be quantal, glutamatergic (Dulon et al., 2009; Spaiardi, Marcotti et al., 2020; Spaiardi, Tavazzani et al., 2020).

We recently investigated the exocytosis of synaptic vesicles in type I and type II mouse utricular hair cells by monitoring real-time changes in ΔC_m during whole-cell patch-clamp recordings (Spaiardi et al., 2022). With this technique electrical measurements of the ΔC_m of a single cell are used to follow the changes in cell-surface area associated with membrane addition during exocytosis, and membrane retrieval during endocytosis (Matthews & Fuchs 2010). We found that both type I and type II hair cells produce a sustained ΔC_m consistent with the exocytosis of synaptic vesicles triggered by the depolarization-induced inflow of Ca^{2+} through the $Ca_V1.3$ Ca^{2+} channels (Spaiardi et al., 2022). The sustained ΔC_m was approximately ten times smaller in type I hair cells compared to that in type II hair cells, suggesting that the exocytosis of synaptic vesicles was a much smaller component of signal transmission in the former (Spaiardi et al., 2022). However a large transient ΔC_m was always present upon repolarization to the holding V_m of −81 mV from depolarizing voltage steps in type I, but not type II hair cells, the amplitude of which did not decrease following the largest depolarizing steps that elicit little or no I_{Ca} (Spaiardi et al., 2022). Furthermore the transient ΔC_m was still present in $Ca_V1.3^{-/-}$ mice, which express a relatively small residual I_{Ca} (19% compared to WT mice; Manca et al., 2021), whereas the sustained ΔC_m (exocytosis) was absent (Spaiardi et al., 2022). Finally the transient ΔC_m reversed direction upon repolarization to the holding V_m of −81 mV from hyperpolarized voltages steps (Spaiardi et al., 2022). The nature of the transient ΔC_m, however, was not elucidated, which is the aim of the present study.

We found that the transient ΔC_m in type I hair cells was not affected by intracellular Ca^{2+} chelation by high EGTA, conclusively establishing its insensitivity to intracellular Ca^{2+}. Moreover, its amplitude, sign and kinetics correlated with $G_{K,L}$ activation or deactivation, suggesting it was generated by intramembrane charges translocation associated with gating of K,L channels. Finally we found that the amplitude of the transient ΔC_m was significantly reduced despite a similar $G_{K,L}$ in $Caspr^{-/-}$ mice, which because of the lack of the core protein of its septate-like junction, Caspr, at the type I hair cell-calyx synapse, have a much larger synaptic cleft (Sousa et al., 2009).

The present results are consistent with the afferent calyx enclosing a high-resistance intercellular compartment in series with the hair cell membrane resistance, which amplifies the capacitance signal generated by the gating of K,L channels. It cannot, however, exclude a physiological mechanism linking the K,L channel gating with postsynaptic elements by the Caspr protein, or by protein/s aggregated there, which could be not expressed, washed away or misplaced in the lack of this junction.

Methods

Ethical approval

Animal experimental work was licensed by the UK Home Office under the Animals (Scientific Procedures)

Paolo Spaiardi is a tenure track assistant professor in the Department of Biology and Biotechnology 'Lazzaro Spallanzani' at the University of Pavia. He completed his PhD in neuroscience and physiology at the same university. His research focuses on the neurophysiological and biophysical mechanisms underlying the functioning of the vestibular system and areas of the central nervous system, such as the parahippocampal cortices.

Act 1986 (PCC8E5E93 and PP1481074) and was approved by the University of Sheffield Ethical Review Committee (180626_Mar). Animals of either sex were killed by cervical dislocation followed by decapitation in accordance with UK Home Office regulations.

Animals and tissue preparation

Vestibular hair cells were studied in acutely dissected C57B/6N mouse utricles from postnatal day 18 (P18) to P28, where the day of birth is P0. This is an age when the maturation of the sensory vestibular epithelium is considered complete (Burns & Stone, 2017; Burns et al., 2012). For some experiments utricles were obtained from *Caspr*$^{+/-}$ and *Caspr*$^{-/-}$ mice, aged P19-39. Caspr mice were a kind gift from Prof. Elior Peles, Weitzmann Institute of Science (Rehovot, Israel) (for details on the Caspr mice see Gollan et al., 2003).

Mouse utricles were dissected in the following extracellular solution (in mM): 135 NaCl, 5.8 KCl, 1.3 $CaCl_2$, 0.9 $MgCl_2$, 0.7 NaH_2PO4, 5.6 D-glucose, 10 Hepes-NaOH. Sodium pyruvate (2 mM), MEM amino acids solution (50×, without L-glutamine) and MEM vitamins solution (100×) were added from concentrates (Fisher Scientific, Loughborough Leicestershire, UK); the pH was adjusted to 7.5 (osmolality about 308 mmol/kg). The dissected utricles were transferred to a microscope chamber, immobilized using a nylon mesh fixed to a stainless-steel ring and continuously perfused with the above extracellular solution. The utricles were observed with an upright microscope (Nikon FN1, Tokyo, Japan) equipped with Nomarski differential interference contrast optics (X60 water immersion objective and X15 eyepieces).

Whole-cell electrophysiology

All whole-cell patch-clamp recordings were performed at near body temperature (34°C–37°C) using an Optopatch amplifier (Cairn Research Ltd, Faversham, UK). Patch pipettes (3–4 MΩ) were pulled from soda glass capillaries (Hilgenberg, Malsfeld, Germany) and coated with surf wax (Mr. Zogs Sex Wax, Carpinteria, CA, USA) to minimize the fast capacitance transient of the patch pipette. Hair cells from the striola or extrastriolar regions of the mouse utricle were used in this study. Access to the hair cells was gained by using a 4 µm tip borosilicate glass pipette filled with a normal extracellular solution and connected to a syringe to apply light suction and pressure to clean the cell membrane prior to patching. As previously reported (e.g. Spaiardi et al., 2017) a patch pipette was used to remove the tissue debris above the targeted hair cell prior to seal it. The calyx had to be pierced to gain access to the hair cell basolateral membrane (see Fig. 1). It is likely that both the outer and inner calyx membrane below the patch pipette were aspirated because of the negative pressure used to seal and to rupture the hair cell membrane. No substantial differences between WT and KO were noticed, possibly because the above procedure was rather variable among experiments.

For Ca^{2+} current (I_{Ca}) and capacitance measurements (described below), K^+ currents were minimized using a CsGlutamate-based intracellular solution containing (in mM): 110 Cs-glutamate, 20 CsCl, 3 $MgCl_2$, 1 EGTA-CsOH, 5 Na_2ATP, 0.3 Na_2GTP, 5 Hepes-CsOH, 10 Na_2-phosphocreatine (pH 7.3 with CsOH; about 295 mmol/kg). Since $G_{K,L}$ is rather permeable to Cs^+ (Rennie & Correia 2000; Rüsch & Eatock, 1996; Spaiardi et al., 2017), this allowed us to identify type I hair cells since type II hair cells do not have $G_{K,L}$. The residual $I_{K,L}$ plus I_h, which are not blocked by intracellular Cs^+ (Fig. 7), were then blocked by locally perfusing the hair cells with an extracellular solution containing TEA and 4-AP (in mM): 110 NaCl, 5.8 CsCl, 1.3 $CaCl_2$, 0.9 $MgCl_2$, 0.7 NaH_2PO_4, 5.6 D-glucose, 10 Hepes, 30 mM TEA, and 15 mM 4-AP (pH adjusted to 7.5 with NaOH, osmolality about 312 mmol/kg).

Voltage protocols and data acquisition were controlled by pClamp software using a Digidata 1440A board (Molecular Devices, San Jose, CA, USA). Voltage-clamp recordings were low-pass filtered at 2.5 kHz (8-pole Bessel) and sampled at 5 kHz or 50 kHz. Data analysis was performed using Clampfit (Molecular Devices, USA) and Origin software (OriginLab, Northampton, MA, USA). Membrane potentials were corrected for the voltage drop across the series resistance (R_s) and a liquid junction potential of −11 mV between the Cs-Glutamate-based pipette solution and bath solution. The isolated Ca^{2+} current recordings were corrected offline for the linear leak current (I_{leak}) typically calculated between −81 mV and −71 mV.

Membrane capacitance measurements

Real-time measurement of cell membrane capacitance was performed with the 'track-in' circuitry of the Optopatch amplifier (Johnson et al., 2002, 2005) using a 4 kHz sine wave voltage command (13 mV RMS amplitude) applied at the holding V_m of −81 mV, or −131 mV in some experiments. The exocytosis of synaptic vesicles was measured as the change ΔC_m produced by Ca^{2+} influx elicited by 200 ms depolarizing voltage steps of variable size. The sine wave used to measure real-time C_m was interrupted for the duration of the voltage steps. The capacitance signal from the Optopatch was amplified (50×), filtered at 250 Hz and sampled at 5 or 50 kHz. The ΔC_m as a function of cell membrane voltage was obtained as the difference between the mean baseline capacitance

signal and that measured over a 200 ms, or greater, period after each depolarizing voltage step. To investigate the Ca^{2+}-dependence of the ΔC_m changes (Fig. 2) we used the same CsGlutamate-based intracellular solution but increased the EGTA concentration to 10 mM, with an equimolar reduction in glutamate concentration.

Statistical analysis

Differences in the mean were compared for statistical significance with an unpaired Student's two-tailed *t* test. For comparisons of multiple groups of data, we used a one-way ANOVA, or for two groups of multiple data sets we used a two-way ANOVA, both followed by a Sidak

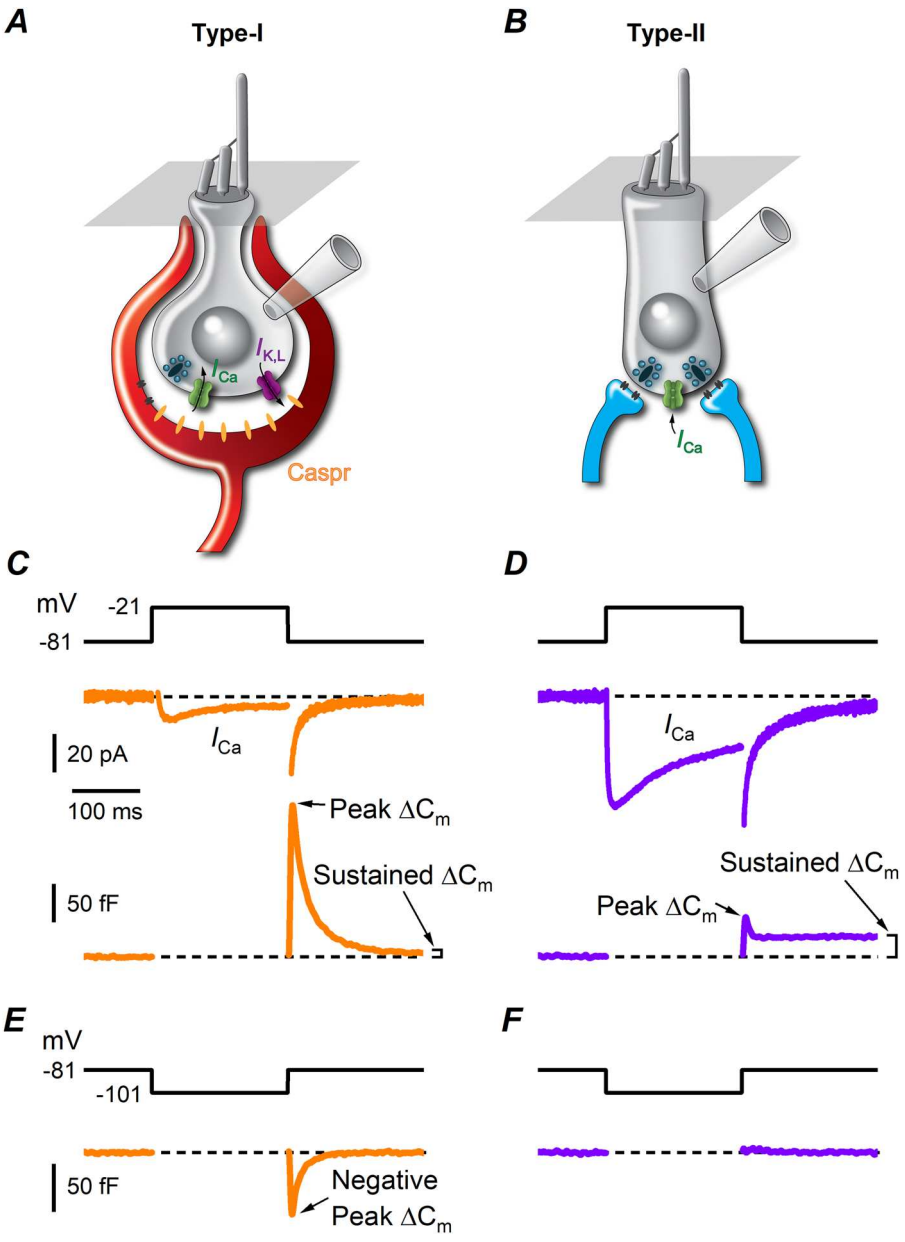

Figure 1. The typical I_{Ca} and ΔC_m recorded from a type I or a type II hair cell
A, *B*, cartoon of the whole-cell recording configuration from a type I or a type II hair cell. Note that the afferent nerve calyx must be pierced to seal the hair cell basolateral membrane. *C*, *D*, representative voltage-clamp recordings with the CsGlutamate-based intracellular solution and the extracellular solution containing TEA and 4-AP to block K^+ channels (see Methods). From the V_{hold} of −81 mV, the voltage steps to −21 mV elicited a small or large inward I_{Ca} in type I or type II hair cells, while no current were elicited in response to the voltage step of −101 mV in either cell type. *E*, *F*, corresponding ΔC_m upon repolarization to holding V_m. While the sustained ΔC_m was significantly larger in type II than in type I hair cells, the latter showed a much larger transient ΔC_m. Note that the sign of the transient ΔC_m elicited in type I hair cells reversed upon repolarization to holding V_m from −101 mV.

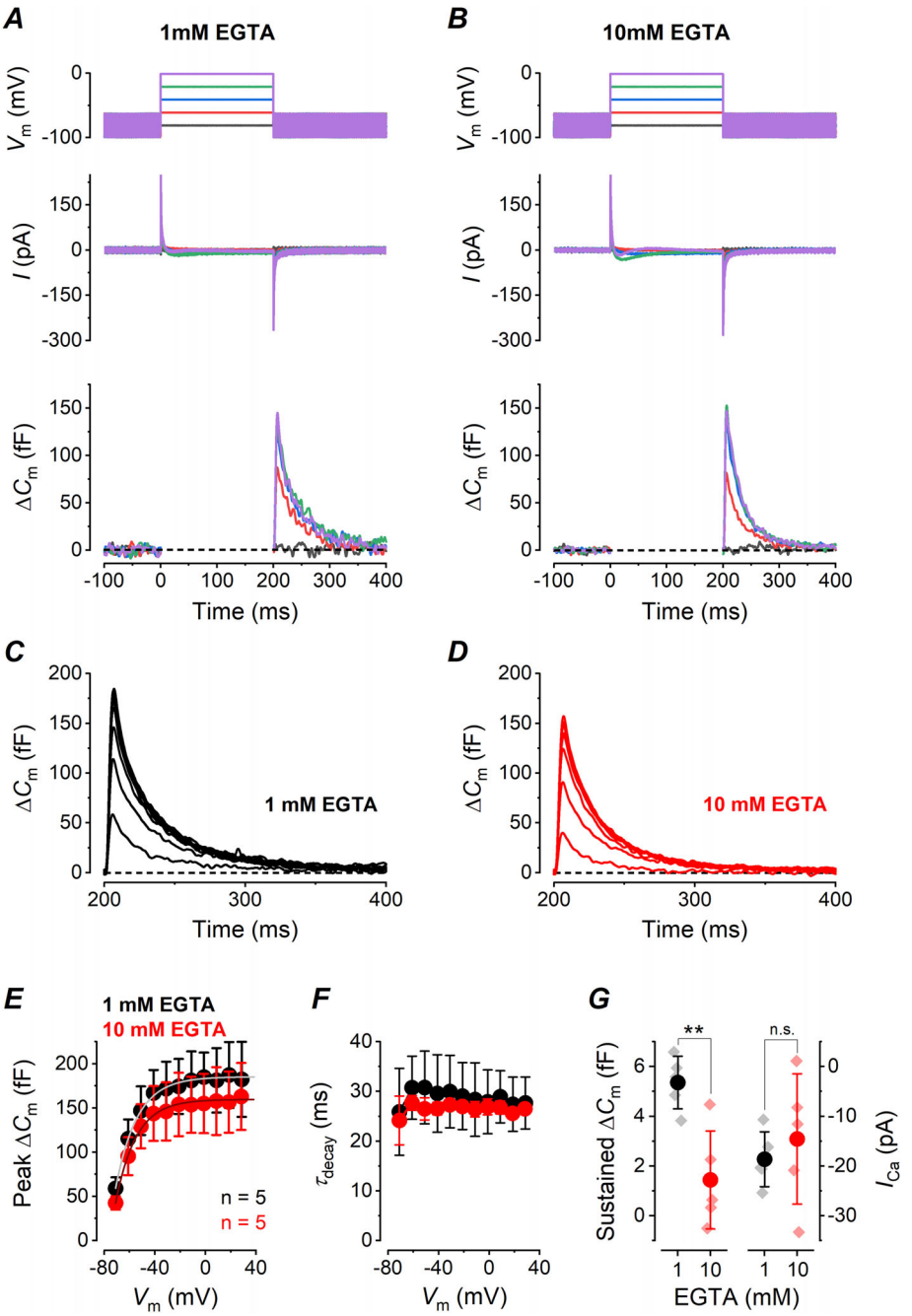

Figure 2. Ca^{2+} current and exocytosis in wild-type (WT) vestibular type I hair cells of mature mouse utricles with 1 or 10 mM intracellular EGTA
A, sample I_{Ca} (top panel) and corresponding ΔC_m (bottom panel) responses recorded from a type I hair cell with 1 mM intracellular EGTA. Recordings were obtained in response to 10 mV voltage steps (200 ms) from the V_{hold} of −81 mV ranging from −101 to 47 mV and returning to −81 mV, as from the voltage protocol shown above I_{Ca} traces. The thick continuous line of the voltage protocol, interrupted for the duration of the voltage steps, consists of a 4 kHz sine wave *B*, sample I_{Ca} (top panel) and corresponding ΔC_m (bottom panel) responses recorded from a type I hair cell with 10 mM intracellular EGTA. Same voltage protocol as in *A*. Despite the presence of I_{Ca}, the sustained ΔC_m responses were almost completely abolished by EGTA, but transients ΔC_m remained evident. *C*, average ΔC_m response recorded with 1 mM intracellular EGTA. *D*, average ΔC_m response recorded with 10 mM intracellular EGTA. ΔC_m recordings were performed in the presence of TEA and 4-AP. *E*, mean peak ΔC_m as a function of voltage in 1 or 10 mM EGTA. *F*, decay time constant of the peak transient ΔC_m in 1 mM or 10 mM EGTA. *G*, average sustained ΔC_m (re: left vertical axis) and I_{Ca} (re: right vertical axis) measured in 1 or 10 mM EGTA in the recording pipette. Only values for steps from −81 mV to −21 mV are shown. The mean sustained ΔC_m resulted significantly smaller in 10 mM intracellular EGTA compared with 1 mM EGTA, whereas I_{Ca} amplitude was similar in either condition.

multiple comparison post test. Mean values are quoted ± s.d.; $P < 0.05$ indicates statistical significance.

Results

Vestibular hair cells are the sensory receptors of the vestibular system that convert head movements into neuronal activity via the release of neurotransmitter onto their synaptic contacts. The relation between the inward Ca^{2+} current (I_{Ca}) and exocytosis has been investigated in mature vestibular type I and type II hair cells using single-cell patch-clamp recordings in *ex-vivo* explants of mouse vestibular organs (Dulon et al., 2009; Spaiardi, Marcotti et al., 2020; Spaiardi, Tavazzani et al., 2020; Spaiardi et al., 2022; Vincent et al., 2014). Although the exact functional role of type I and type II hair cells is currently uncertain, the cells are very different. The main features of type I and type II hair cells are summarized in Fig. 1. Type I hair cells are characterised by the presence of a single calyx afferent terminal that almost completely encases the basolateral membrane of the cell (Fig. 1*A*; Lysakowski & Goldberg, 2004; Wersäll, 1956). By contrast, type II hair cells are contacted by multiple small bouton-like afferent terminals that are like those on auditory hair cells (Fig. 1*B*; Lysakowski & Goldberg, 2004). Type I hair cells are also characterized by the expression of $I_{K,L}$ that is not present in type II hair cells (Correia & Lang, 1990; Rennie & Correia, 1994; Rüsch & Eatock, 1996). Both hair cell types express a voltage-dependent I_{Ca}, mainly carried by $Ca_V1.3$ Ca^{2+} channels, which is much smaller in type I than in type II hair cells (Fig. 1*C* and *D*; Manca et al., 2021; Spaiardi et al., 2022). Consistent with their larger I_{Ca}, type II hair cells show a much larger amount of synaptic vesicle exocytosis than that seen in type I hair cells, which is evident from the 10 times larger sustained ΔC_m recorded in these cells (Fig. 1*C* and *D*). Type I hair cells, however, have a large positive transient ΔC_m component that is always present upon repolarization to the holding V_m from depolarized potentials, which is much smaller in type II hair cells (Fig. 1*C* and *D*). The transient ΔC_m in type I hair cells becomes negative upon returning to the holding V_m from voltage steps to more hyperpolarised potentials, which does not occur in type II hair cells (Fig. 1*E* and *F*). In contrast to the Ca^{2+}-dependence of the sustained ΔC_m, which is indicative of synaptic vesicle exocytosis, the size of the transient ΔC_m did not vary based on I_{Ca} amplitude and was still present, and apparently unaffected, in $Ca_V1.3^{-/-}$ mice (Spaiardi et al., 2022).

The above findings suggest that the large transient ΔC_m recorded from type I hair cells does not depend upon Ca^{2+} entry through voltage-gated $Ca_V1.3$ Ca^{2+} channels. However since a small residual I_{Ca} was still present in $Ca_V1.3^{-/-}$ hair cells (Manca et al., 2021), whose molecular nature remains to be elucidated, and to gain more information about the Ca^{2+}-dependence of ΔC_m in type I hair cells, we tested the effect of intracellular EGTA at a concentration of 1 and 10 mM. EGTA is a Ca^{2+} chelator that has been widely used to probe the coupling between Ca^{2+} channels and vesicular Ca^{2+} sensors for neurotransmitter release (Augustine et al., 2003; Neher, 1998). Representative current traces and the corresponding ΔC_m obtained in the presence of either 1 or 10 mM intracellular EGTA from a type I hair cell are shown in Fig. 2*A* and *B*, respectively – the average ΔC_m from all cells are shown in Fig. 2*C* and *D*. The average values for the peak amplitude and decay time constant (τ_{decay}) of the transient ΔC_m elicited upon repolarization to the holding V_m of −81 mV following depolarized voltage steps in 1 and 10 mM EGTA are shown in Fig. 2*E* and *F*, respectively. Although there was an overall difference in the size of the peak transient ΔC_m and τ_{decay} at the two EGTA concentrations (two-way ANOVA; peak ΔC_m $P = 0.0002$; τ_{decay} $P = 0.0201$), post tests revealed no significant difference between values at individual V_m (Sidak multiple comparisons post test $P > 0.05$ for each pair of values). Since we will show below that the transient ΔC_m correlates with $G_{K,L}$ activation, it is presumable that the above overall difference reflects the large variability in $G_{K,L}$ voltage-dependence among type I hair cells (Hurley et al., 2006). Maximal values for the peak ΔC_m were obtained by fitting the plot of ΔC_m *versus* V_m with a single exponential function (Fig. 2*E*), and they were statistically similar in 1 mM and 10 mM EGTA (1 mM: 188 ± 33 fF, $n = 6$; 10 mM: 160 ± 35 fF, $n = 5$; $P = 0.21$ Student's unpaired *t* test). The independence of the transient ΔC_m from intracellular Ca^{2+} indicates that it is related to something other than presynaptic vesicle fusion. By contrast, the sustained component of the ΔC_m response in type I hair cells, which is evident after the transient component, reflects synaptic vesicle exocytosis in these cells (Spaiardi et al., 2022). We therefore investigated the effect of high intracellular EGTA on exocytosis in these cells by measuring the sustained ΔC_m following a voltage step to −21 mV, which maximally activates I_{Ca} (Spaiardi et al., 2022). While the size of the peak inward I_{Ca} was not significantly different in 1 or 10 mM EGTA, the sustained ΔC_m was significantly reduced (Fig. 2*G*; I_{Ca} $P = 0.54$; ΔC_m $P = 0.0045$, unpaired *t* test), indicating that synaptic vesicle exocytosis is largely uncoupled from I_{Ca} in the presence of high intracellular EGTA. Since we measure exocytosis as the sustained ΔC_m towards the end of the recordings after the transient ΔC_m, it is possible that this large transient component masks additional synaptic vesicle exocytosis within the first few 100 ms following the voltage steps, which we cannot discern. This aspect is important because a fast-transient exocytosis of glutamate might contribute to the phasic response recorded from calyx afferents innervating type I hair cells (Songer & Eatock, 2013). Although post-synaptic AMPA receptors,

which are expressed at the calyx terminal (Sadeghi et al., 2014), can generate transient postsynaptic responses because of their rapid desensitization, intrinsically transient glutamate exocytosis despite a sustained I_{Ca} has been reported previously at the ribbon synapse of retinal bipolar cells (Singer & Diamond, 2003). To separate the synaptic from the non-synaptic component of the ΔC_m response, we subtracted the ΔC_m trace at a V_m where Ca^{2+}-driven exocytosis was negligible from the one where it was maximal, but where the transient ΔC_m was approximately the same size and time course. In type I hair cells, the transient ΔC_m had approximately maximal amplitude and kinetics following voltage steps of −41 mV and above (Fig. 2*E* and *F*), while the peak I_{Ca} and sustained ΔC_m occurred at −21 mV (Fig. 2*G* and Spaiardi et al., 2022).

Therefore we used the ΔC_m trace recorded after a voltage step to either −41 mV or +19 mV to subtract from that at −21 mV, since both potentials activate a much smaller I_{Ca} and exocytosis in type I hair cells (Spaiardi et al., 2022) and are at opposite sides of the peak response at −21 mV, in 1 mM and 10 mM EGTA (Fig. 3*A* and *B*, respectively). The average ΔC_m resulting from the subtraction of the trace at −41 mV from that at −21 mV showed the absence of the large transient ΔC_m component in 1 mM (Fig. 3*C*) and 10 mM EGTA (Fig. 3*D*), while there was a sustained ΔC_m after the voltage step in 1 mM EGTA (Fig. 3*C*, 3.8 ± 1.2 fF, $n = 5$), that was not present in 10 mM EGTA (Fig. 3*D*, 0.2 ± 1.9 fF, $n = 5$: $P = 0.0066$, unpaired *t* test). Similar results were obtained for the subtraction of the ΔC_m at +19 mV from −21 mV (Fig. 3*E*, 1 mM EGTA: 3.6 ± 1.3 fF, $n = 5$; Fig. 3*F*, 10 mM EGTA: 0.3 ± 1.7 fF, $n = 5$: $P = 0.0085$, unpaired *t* test). The size of the sustained ΔC_m in 1 mM EGTA isolated from both subtractions was not significantly different from that measured after the transient ΔC_m (Fig. 2*G*) or from that previously reported (Spaiardi et al., 2022; $P = 0.6$, one-way ANOVA). Moreover the sustained ΔC_m in 10 mM EGTA obtained with and without subtraction

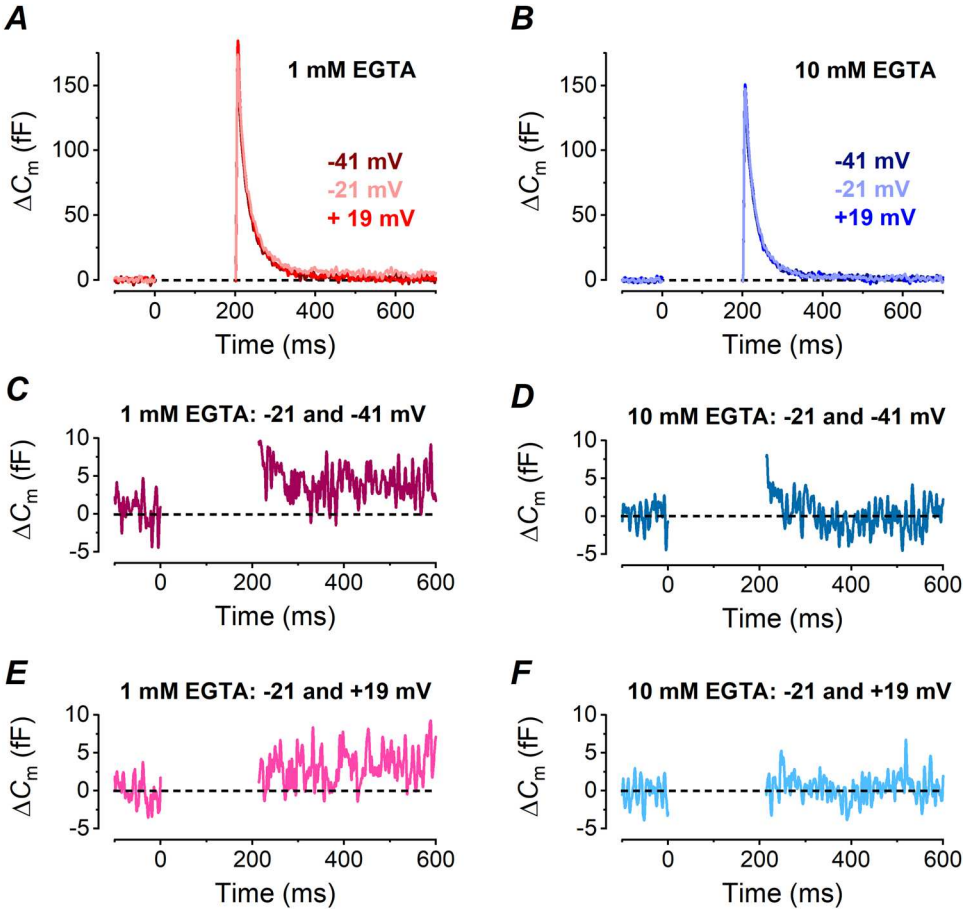

Figure 3. Peak and sustained ΔC_m in wild-type (WT) vestibular type I hair cells are differently sensitive to 1 mM or 10 mM intracellular EGTA
A, *B*, ΔC_m recorded after a voltage step to either −41, −21 or +19 mV in 1 or 10 mM intracellular EGTA, respectively. *C*, *D*, average differential trace obtained by subtracting ΔC_m recorded at −41 mV from that recorded at −21 mV in 1 mM or 10 mM intracellular EGTA, respectively. *E*, *F*, average differential trace obtained by subtracting ΔC_m recorded at +19 mV from that recorded at −21 mV in 1 mM or 10 mM intracellular EGTA, respectively.

were not significantly different as well ($P = 0.5$, one-way ANOVA). In conclusion the ΔC_m due to Ca^{2+}-dependent exocytosis in type I hair cells is fully uncoupled by 10 mM intracellular EGTA; moreover the large transient ΔC_m is non-synaptic, is not dependent on Ca^{2+} entry and does not mask any exocytotic component that is larger than the one measured after the transient. Instead the size of the transient ΔC_m is non-linearly dependent on V_m (Fig. 2*E*) and peaks in the negative direction in response to a return to the holding V_m of −81 mV following a voltage step to a more hyperpolarized V_m (Fig. 1*E*; Spaiardi et al., 2022). The negative transient ΔC_m is unlikely to correspond to endocytosis since this also requires elevations in Ca^{2+} (Yamashita et al., 2010), which does not occur at these very negative potentials. Since the transient ΔC_m changes non-linearly with the V_m and increased in size up to around −41 mV (Fig. 2*E*), a voltage at which $G_{K,L}$ activation nearly saturates (Spaiardi et al., 2020), it is possible that it is generated by the gating of $G_{K,L}$.

The large transient ΔC_m in type I hair cells correlates with the level of $G_{K,L}$ activation

The main outward K^+ conductance in type I mammalian vestibular hair cells is $G_{K,L}$, which is absent from type II cells, activating at very negative V_m (−100 mV) and being about half maximally activated at −80 mV (see Spaiardi et al., 2017 for characterization of $G_{K,L}$ activation curve). The $G_{K,L}$ channel gating transiently displaces charges from one side of the membrane to the other that sums with those displaced by the sinusoidal stimulus used to measure C_m (see eqn (4) below) that could cause the transient increase in C_m illustrated in Figs 1–3. This transient ΔC_m could be useful for investigating channel gating (or, in general, any protein rearrangement involving a charge displacement in a membrane protein) that can be especially prominent for ion channels characterized by prolonged tail currents after excitation with depolarizing pulses, as is the case for $G_{K,L}$. Several studies have taken advantage of ΔC_m measurements to detect changes in the number or mobility of any charged group residing within the electric field of the membrane, such as ion channel gating (Kilic & Lindau 2001) or membrane transporters (Lu et al., 1995). A large transient ΔC_m, unrelated to Ca^{2+}-dependent exocytosis, has been reported in adrenal chromaffin cells and was shown to be due to Na^+ channel gating charge movement associated with channel de/inactivation (Horrigan & Bookman, 1994), the magnitude and time course of which were like that seen in type I vestibular hair cells. To investigate the relationship between the $G_{K,L}$ gating and the transient ΔC_m, the latter was measured upon returning the same type I hair cell from different potentials to the holding V_m of −81 mV, where $G_{K,L}$ is half activated (Fig. 4*A*, bottom panel), or to V_{hold} of −131 mV, where $G_{K,L}$ is fully deactivated (Fig. 4*B*, bottom panel). Average ΔC_m traces for the two holding voltages of −81 mV and −131 mV are shown in Fig. 4*C* and *D*, respectively. The curves describing the voltage dependence of the peak ΔC_m upon returning to −81 mV or −131 mV are shown in Fig. 4*E* (black or red dots, respectively). The peak ΔC_m responses elicited from −131 mV were similar to the $G_{K,L}$ activation curve (Fig. 4*E*, blue curve). This indicates that the transient ΔC_m could be generated by the translocation across the hair cell membrane of the voltage sensor gating charge, associated with K,L channel closure upon repolarizing to the V_{hold} of −131 mV. Consistent with this hypothesis, the size of the ΔC_m transients from voltages more negative than −70 mV to V_{hold} of −131 mV (Fig. 4*E*, red dots) was larger than the ones to V_{hold} of −81 mV (Fig. 4*E*, black dots), due to the larger number of channels that close for the former voltage step (moving a larger number of gating charges) with respect to the latter. The values of the transient ΔC_m upon repolarization to either V_{hold} of −81 mV or −131 mV from voltages are more depolarized than −51 mV overlap (Fig. 4*E*, black and red dots, respectively), because at these voltages $G_{K,L}$ is fully activated. As expected the amplitude of the transient ΔC_m saturates at voltages where all the gating charges of $G_{K,L}$ are supposedly in the open or in the closed positions. The presence of a transient ΔC_m at voltages where $G_{K,L}$ is not yet active (−100 mV) in Fig. 4*E* is not an incongruity, since $G_{K,L}$ could be well described by an allosteric Markov gating model showing multiple closed and open states (Spaiardi et al., 2017). According to this model the gating particles are expected to move at voltages just below the threshold for opening the channels, due to the redistribution of the channels among the closed states, resulting in a curve for the gating charge (Q), that is, in a curve for the amplitude of the transient ΔC_m, that is, voltage, shifted to the left (i.e. toward more hyperpolarized voltages) compared to $G_{K,L}$ activation curve (Armstrong, 1981; see Catacuzzeno et al., 2023 for a recent review). On the contrary, the earlier saturation of the Q curve in respect to the $G_{K,L}$ one for voltages between −60 and −30 mV is likely due to the relatively slow activation kinetics of $G_{K,L}$, since the 200 ms steps used here are too brief to let the $G_{K,L}$ to reach the steady-state activation (see, e.g. Fig. 7 in Spaiardi et al., 2017). Since all K,L channels are closed at −131 mV, there would be no gating charge movements for voltage steps to more negative potentials, and no transient ΔC_m was indeed recorded at −141 mV (Fig. 4*E*, red dots). Also since additional K,L channels will open upon stepping, for instance, from −91 mV to −81 mV, which will produce a movement of the gating charges in the opposite direction to their closure, a negative transient ΔC_m is expected, as it was indeed detected (Fig. 4*E*, black dots). Finally the τ_{decay} of the transient ΔC_m elicited upon repolarization from each test potential to the holding V_m of −131 mV was

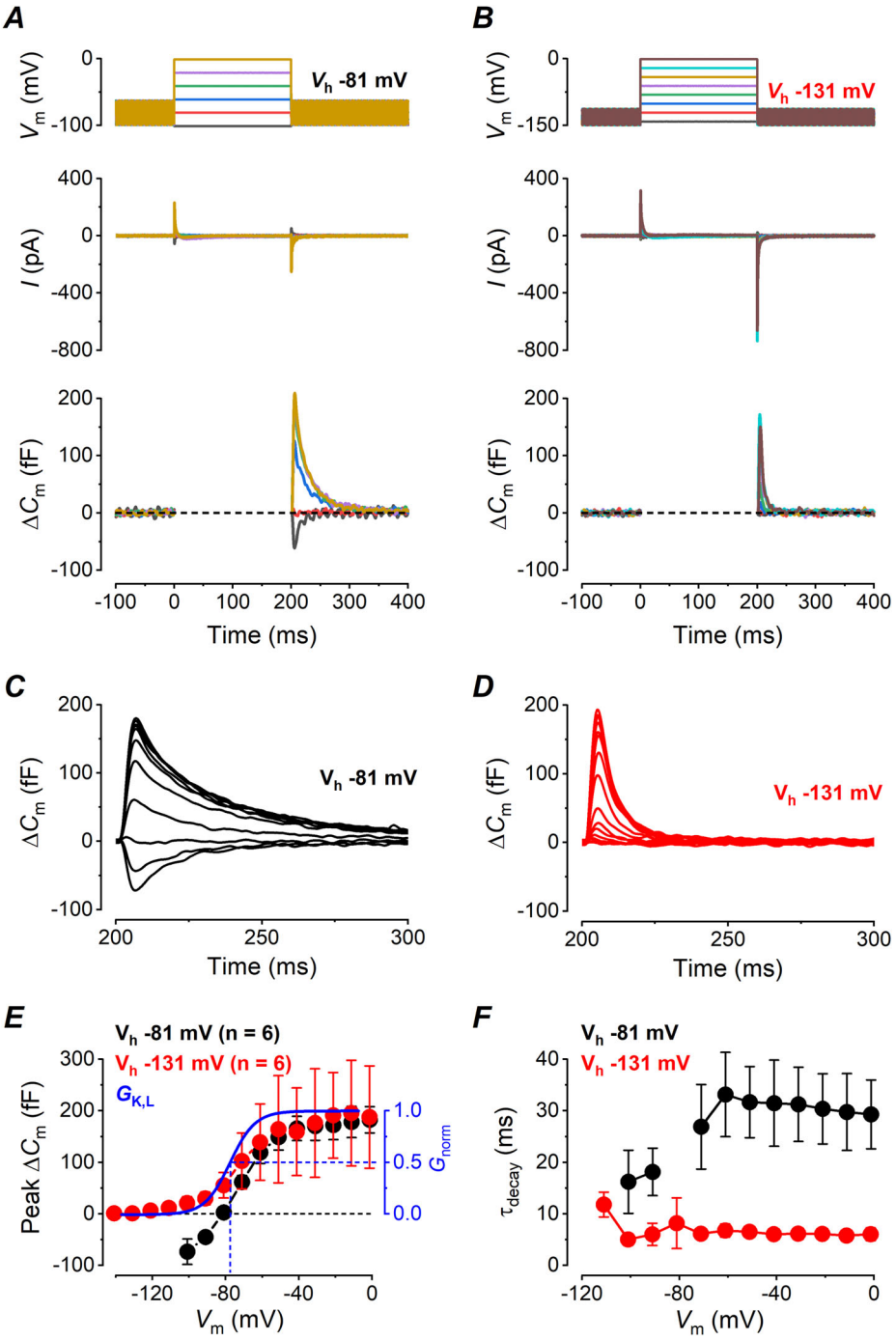

Figure 4. Transient ΔC_m in wild-type (WT) vestibular type I hair cells of mature mouse utricles obtained by using different holding V_m
A, sample I_{Ca} (top panel) and corresponding ΔC_m (bottom panel) responses recorded from a type I hair cell in response to 20 mV voltage steps (200 ms) from holding V_m of −81 mV ranging from −101 to −1 mV and returning to −81 mV, as from the voltage protocol shown above I_{Ca} traces. *B*, sample I_{Ca} (top panel) and corresponding ΔC_m (bottom panel) responses recorded from a type I hair cell in response to 20 mV voltage steps (200 ms) from holding V_m of −131 mV ranging from −141 to −1 mV and returning to −131 mV, as from the voltage protocol shown above I_{Ca} traces. *C*, average ΔC_m recorded upon repolarization to −81 mV following voltage steps ranging from −101 to −1 mV. *D*, average ΔC_m recorded upon repolarization to −131 mV following voltage steps ranging from −141 mV to −1 mV. *E*, voltage-dependence of the mean peak transient ΔC_m responses measured upon returning to the holding V_m of −81 or −131 mV. The blue curve indicates the normalized activation curve for $G_{K,L}$, as from Spaiardi et al. (2017) (half activation voltage: −79.65 mV). *F*, mean τ_{decay} obtained by the same pool of cells as in *E*.

Table 1. Parameters of equations

Abbreviation	Meaning	Value	Citations
r_h	Cell radius	2.5 µm	Govindaraju et al. (2022)
s_c	Synaptic cleft length	0.02 µm	Govindaraju et al. (2023)
Vol_{cl}	Cleft volume	1.2 µm^3	**eqn (6)**
f	Fraction of basal membrane enwrapped by calyx	0.75	Govindaraju et al. (2023)
ρ	Extracellular solution resistivity	100 Ω cm	Textbook value
R_m	Cell input resistance	≈3 GΩ	Experimental data
R_s	Series resistance	≈10 MΩ	Experimental data
R_c	Calyceal synaptic cleft resistance	≈40 MΩ	Estimated
C_m	Cell capacitance	≈10 pF	Experimental data
ΔC_m	Cell capacitance change		Variable
I	Current		Variable
ΔI	Current change		Variable
E_s	Voltage stimulus		Variable
ν	Sinusoid frequency of E_s		Variable
θ	phase angle between ΔI and V_s		Variable
n	change of cleft K^+ concentration moles/s		Variable
e	Elementary charge	1.602×10^{-19} C	Physical constant
N_o	Avogadro number	6.022×10^{23} mol^{-1}	Physical constant

significantly faster than that elicited upon repolarization to −81 mV ($P < 0.0001$; two-way ANOVA; Fig. 4*F*), which is consistent with the faster decay of $I_{K,L}$ for stronger repolarizations (Spaiardi et al., 2017). All the results so far described strongly indicate that the transient ΔC_m can be considered, albeit within certain limits, a readout of the $G_{K,L}$ gating.

Does the calyx play a role in the large transient ΔC_m?

The large amplitude of the transient ΔC_m requires careful consideration of the relative amplitudes of the hair cell input resistance, R_m, and the series resistance, R_s, because large artefactual transient changes in membrane capacitance can be elicited by substantial changes in R_m if R_m and R_s are of comparable amplitude (Barnett & Misler, 1997). Indeed with a standard K^+-based intracellular solution, R_m in type I hair cells, because of the large $G_{K,L}$, is of similar amplitude to that of R_s (around 10 MΩ; Contini et al., 2012). However substituting intracellular K^+ with Cs^+ and adding blockers of K^+ channels, as done here, increased the value of R_m of type I hair cells to 3.06 ± 1.00 GΩ ($n = 25$, measured by a brief voltage pulse between −91 mV and −81 mV), similar to that of type II hair cells (2.56 ± 1.00 GΩ, $n = 25$, $P = 0.37$; Spaiardi et al., 2020b). Indeed even the most depolarized voltage steps elicited outward (Cs^+) current ≤ 100 pA in either cell type (Fig. 2*A* and *B*), meaning that R_m was at all voltages ≥ 1 GΩ, i.e. much larger than the typical R_s values. Therefore the dramatic difference in the amplitude of the transient ΔC_m (196.0 ± 46.8 fF *vs.* 32.7 ± 23.4 fF in the same type I and type II hair cells, measured at −41 mV) cannot be explained by differences in R_m or R_s between the two hair cell types. However an additional R_s should be considered here for recordings from type I hair cells, that is the resistance of the calyceal synaptic cleft, R_c, as follows.

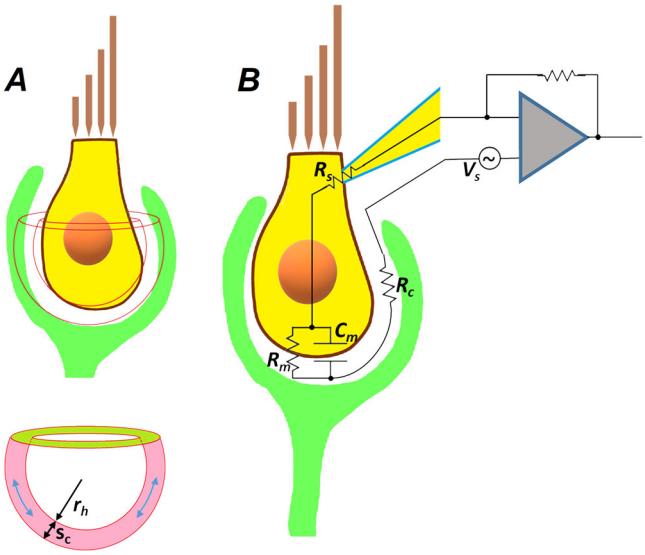

Figure 5. The calyx cleft contribution to the hair cell electrical measurements
A, geometry of the calyx: the hair cell basal pole is approximated to a sphere of radius r_h; s_c is the thickness of the synaptic cleft (approximated to a sphere as well). *B*, the equivalent circuit model for a whole-cell recorded type I hair cell that measures current flowing in response to a voltage stimulus V_s, consisting of the series (access) resistance R_s, the cell membrane resistance R_m, the cell membrane capacitance C_m and the cleft resistance R_c.

The basolateral membrane of type I hair cells is almost completely enveloped by the single giant afferent calyx nerve terminal (Figs 1*A* and 5), and early models (Goldberg, 1996) recognized that the elongated cleft space could limit the diffusion of ions and provide an increased electrical resistance.

The cleft region can be roughly represented by two hemispheric and concentric shells (Fig. 5*A*, top panel) of radiuses r_h and r_h+s_c (Fig. 5*A*, bottom panel), where r_h is the hair cell radius (2.5 μm; Table 1) and s_c is the synaptic cleft length (0.02 μm; data from Govindaraju et al., 2023), filled with the extracellular solution of resistivity ρ (100 Ω·cm). The current flowing through the hair cell membrane is therefore thought to travel within the calyx cleft (blue arrows in the pink region), along an annular region (whose section is in green in Fig. 5*A* bottom panel). This corresponds to a resistance R_c given by:

$$R_c = \rho \frac{2\pi r_h f}{\pi (r_h + s_c)^2 - \pi {s_c}^2} = \frac{\rho f}{s_c \left(1 + \frac{s_c}{r_h}\right)} \approx \frac{\rho f}{s_c} \quad (1)$$

where f is the fraction of basolateral hair cell membrane (below tight junctions) enwrapped by calyx, that is between 0 (no calyx) and 1 (calyx wraps completely the hair cell): assuming $F = 0.75$ in eqn (1), it results in $R_c \approx$ 38 MΩ. The resistance R_c sums with R_s in the capacitance measurements; therefore, if Z is the impedance of the entire circuit, the current I due to a sinusoidal voltage stimulus V_s of angular frequency $\omega = 2\pi\nu$ (where ν is the sinusoid frequency) will be given by Ohm's law:

$$I = \frac{V_s}{Z} = \left(R_s + \frac{1}{\frac{1}{R_m} + j\omega C_m} + R_c\right)$$

$$V_s = \frac{\frac{1}{R_m} + j\omega C_m}{\frac{R_s+R_c}{R_m} + j\omega C_m (R_s + R_c) + 1} V_s \quad (2)$$

It is impossible to isolate a vector component of I in eqn (2) that is directly proportional to the capacitance. However, since any change in R_c, R_s, R_m or C_m will produce a change ΔI of I, a C_m change (ΔC_m) can be estimated from the induced ΔI (eqn (2)), that was phase-shifted by −90° with respect to the phase angle θ between ΔI and V_s. This ΔI is given by eqn (3):

$$\Delta I = \frac{\partial I}{\partial C_m} \Delta C_m = \frac{j\omega}{\left[\frac{R_s+R_c}{R_m} + j\omega C_m (R_s + R_c) + 1\right]^2} V_s \Delta C_m \quad (3)$$

Since R_m is at least an order of magnitude larger than $R_s + R_c$ (see above), the term:

$$\frac{R_s + R_c}{R_m}$$

can be neglected in eqn (3) that becomes:

$$\Delta I = \frac{j\omega}{\left[j\omega C_m (R_s + R_c) + 1\right]^2} V_s \Delta C_m \quad (4)$$

The phase angle θ of ΔI is given by:

$$\theta = \pi - 2arctan\left[\omega C_m (R_s + R_c)\right] \quad (5)$$

Computer simulations of capacitance changes in whole-cell mode (in a simulated cell with R_s = 10 MΩ, R_m = 1 GΩ and C_m = 6.5 pF) showed that a 10 MΩ increase of R_s gives an artefactual increase of C_m of 50 fF (Fig. 2 of Santos-Sacchi, 2004). Here R_c results in series with R_s (Fig. 5*B*), i.e. R_c just adds to R_s (eqn (4) and 5); therefore, assuming an R_c value about four times larger than R_s (see above) would artefactually alter the C_m measure significantly. Given the large value of R_c, an obvious question is what happens to the C_m measures in the presence of an enlarged cleft calyx synapse: if s_c increased, for example, by twofold (i.e. up to 0.04 μm), then R_c would halve (from ≈38 to ≈19 MΩ; eqn (1)). Note that this artefact occurs also in recordings obtained with the Optopatch amplifier used here that can automatically correct the capacitance recordings of small changes in R_s during the recordings, but it gives artefactually larger capacitance measurements when R_s values approach the R_m ones. In the calyx synapse, the apposed pre- and postsynaptic membranes are kept unusually close by a patterned alignment of proteins resembling a type of intercellular junction that is rare in vertebrates, the septate junction (Sousa et al., 2009). A core molecular component of the septate junction is Caspr, and in *Caspr*$^{-/-}$ mice the separation between the pre- and postsynaptic membranes at the calyx synapse is conspicuously irregular and often increased by an order of magnitude (Sousa et al., 2009). Therefore we measured the amplitude of the capacitive transient in *Caspr*$^{-/-}$ mice to check if it was affected by the R_c reduction occurring in these conditions.

The transient ΔC_m is smaller in *Caspr*$^{-/-}$ type I hair cells

We found that the amplitude of the transient ΔC_m in *Caspr*$^{-/-}$ type I hair cells was significantly smaller than in control (WT and heterozygous mice) cells at every V_m tested ($P < 0.0001$ for pairs of values from −51 mV, Sidak multiple comparisons; Fig. 6*A*–*D*). In particular the maximal value for the peak ΔC_m, obtained by exponential fitting of the ΔC_m *vs.* voltage plots, resulted larger in control type I hair cells (Fig. 6*E*, black dots; 193.2 ± 39.8 pF, $n = 6$) than in *Caspr*$^{-/-}$ cells (Fig. 6*E*, red dots; 121.9 ± 23.6 pF, $n = 11$; $P = 0.0003$, unpaired t test). The τ_{decay} values of the transient ΔC_m for both control and *Caspr*$^{-/-}$ were negligibly voltage-dependent and overlapped at every V_m tested (Fig. 6*F*; $P = 0.8$, two-way

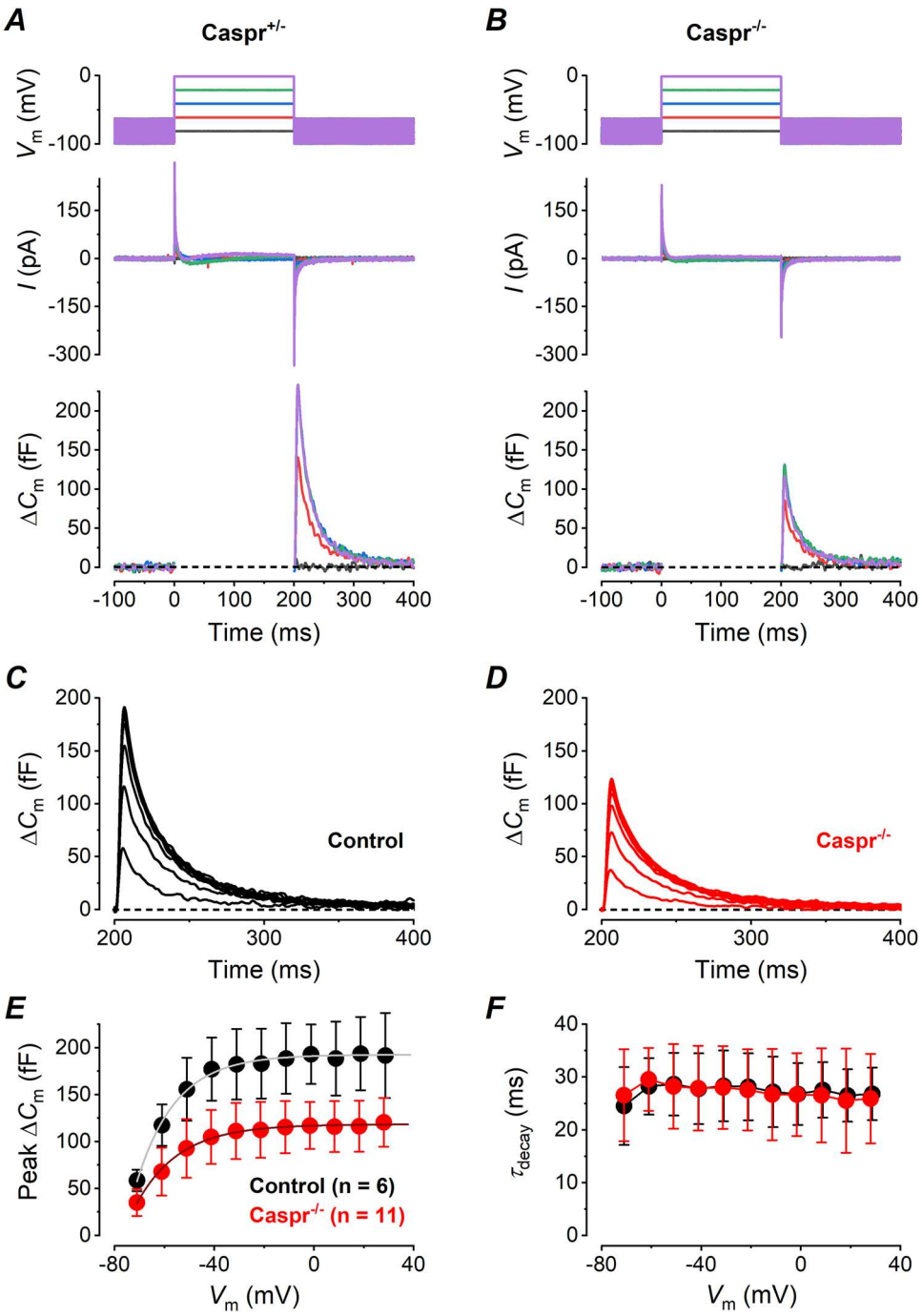

Figure 6. Comparison between control and *Caspr*$^{-/-}$ type I hair cells of mature mouse utricles
A, *B*, representative I_{Ca} (top panel) and ΔC_m (lower panel) recordings from a type I hair cell of a control (*Caspr*$^{+/-}$) and a KO (*Caspr*$^{-/-}$) mouse, respectively. Voltage steps were from −81 to −1 mV in 20 mV increments, from a holding voltage of −81 mV. *C*, *D*, mean transient ΔC_m obtained from six control and 11 *Caspr*$^{-/-}$ type I hair cells, respectively. *E*, plot of the mean transient ΔC_m amplitude *versus* voltage (six control and 11 *Caspr*$^{-/-}$ cells). *F*, mean τ_{decay} of the transient ΔC_m *versus* V_m (six control and 11 *Caspr*$^{-/-}$ cells). Caspr$^{-/-}$ cells (n = 11) were from 4 KO-mice. Control cells were from 1 Caspr Het mouse (n = 2) and two wild type mice (n = 4).

ANOVA, $P > 0.05$ for each pair of values, Sidak multiple comparisons).

The smaller peak transient ΔC_m responses of *Caspr*$^{-/-}$ type I hair cells could be due to a smaller number of K,L channels in these cells compared to controls. To investigate this possibility, we measured the amplitude of the K,L current in the presence of Cs-Glutamate in the intracellular solution before we perfused additional K^+ channel blockers to largely reduce this component. In both *Caspr*$^{-/-}$ and control type I hair cells, upon stepping to about −120 mV there was an initial inward peak current flowing through open K,L channels which then closed (Fig. 7*A*,*B*). From this V_m, the current was inward up to −50 mV and became outward for potentials positive to −40 mV, due to the mixed Cs^+/K^+ current reversal equilibrium in these experimental conditions (Spaiardi et al., 2017). The size of the current through $G_{K,L}$ was similar between *Caspr*$^{-/-}$ and control cells for voltages between −91 mV and −31 mV ($P = 0.054$, two-way ANOVA; voltages more positive than −40 mV were not considered to exclude possible contamination from the delayed rectifier K^+ current which activates positive to −40 mV, see Spaiardi et al., 2017; Fig. 7*C*,*D*). Therefore it is likely that the significantly smaller peak transient ΔC_m in *Caspr*$^{-/-}$ type I hair cells is due to the larger synaptic cleft, i.e., to the smaller R_c and consequently lower amplification of the transient ΔC_m associated with K,L channel gating currents, and not from differences in the numbers or kinetics of K,L channels.

Discussion

Vestibular type I hair cells release glutamate upon Ca^{2+} inflow through voltage-gated $Ca_V1.3$ channels (see Mukhopadhyay & Pangrsic, 2022 for a recent review). Present results show that sustained neurotransmitter exocytosis is nearly abolished in 10 mM intracellular EGTA (Fig. 2*A*, *B* and *G*). Because of its slow forward rate for Ca^{2+} binding, EGTA does not capture Ca^{2+} in very close proximity (tens of nm) of the open Ca^{2+} channel, for which the fast Ca^{2+} chelator BAPTA is required, whereas it chelates Ca^{2+} entered and diffusing at a µm distance from the open Ca^{2+} channels (Neher, 1998). The above results are therefore consistent with Ca^{2+} channels and vesicle release sites being within a microdomain. This is in contrast with previous studies showing that EGTA did not affect (Dulon et al., 2009) or only partially blocked (∼40%; Vincent et al., 2014) exocytosis in mouse type I hair cells, which was conversely fully blocked by BAPTA (both Ca^{2+} chelators tested at 5 mM). It is likely that the difference is due to the mouse age, which in their studies ranged from postnatal day (P)4 to P9, while here it was between P17 and P19. Differences between neonatal and adult mouse vestibular type II hair cells have been reported concerning the Ca^{2+}-dependence of exocytosis, which was linear in neonatal type II hair cells (Dulon et al., 2009), but high order in the adult (>P18) ones (Spaiardi et al., 2022). Several changes are known to occur at the ribbon synapse during hair cell maturation (e.g. Ca^{2+} channel localization, ribbon anatomy; see Pangrsic et al., 2018 and Michanski et al., 2023 for a recent review), which may be responsible for the above different sensitivity to intracellular Ca^{2+} buffers with age.

The large transient ΔC_m recorded in type I hair cells was nearly unaffected by 10mM intracellular EGTA (Fig. 2*A*–*F*), conclusively demonstrating that it does not depend on intracellular Ca^{2+}. On the contrary, the transient ΔC_m correlated with the activation curve of $G_{K,L}$ (the dominant ionic conductance in type I hair cells) – Fig. 4*E*, indicating that it is likely to be generated by the intramembrane movement of the charges associated with the voltage-dependent gating of K,L channels, that are present at very high density (about 150 per µm^2 in rat type I hair cells; Chen & Eatock, 2000). A large transient ΔC_m, unrelated to Ca^{2+} -dependent exocytosis, has been reported in adrenal chromaffin cells and was shown to be due to Na^+ channel gating charge movement associated with channel de/inactivation (Horrigan & Bookman, 1994), the magnitude and time course of which were like that seen in type-I vestibular hair cells. Such transient capacitance signal reflecting Na^+ channel-gating charge movement dibucaine could be cancelled by 200 µM dibucaine that blocks both Na^+ current (I_{Na}) and Na^+ channel-gating charge movement in squid axon (Gilly & Armstrong, 1980), but not by TTX, which blocks I Na but does not immobilize Na^+ channel gating charges. Clearly TEA and 4-AP, here added to the extracellular solution together with intracellular Cs to block $I_{K,L}$, do not immobilize the related gating charges. Finding a drug that immobilizes K,L channel-gates remains an interesting task, also given the recent identification of Kv 1.8 (Kcna10) channel subunits as responsible for carrying $I_{K,L}$ (Martin et al., 2023). A better knowledge of $K_v1.8$ properties is desirable given that *KCNA10* is expressed in the heart, aorta and kidney. Very recently a missense mutation of *KCNA10 h*as been involved in epinephrine provoked long QT syndrome with a familial history of sudden cardiac death (Huang et al., 2023).

The amplitude of the transient ΔC_m was significantly smaller in *Caspr*$^{-/-}$ type I hair cells than in control cells. Caspr is a core molecular component of septate junctions, which in vertebrates are found only in myelin paranodal contacts (Banerjee et al., 2006). These junctions restrict ion movement between the extracellular space confined in the insulated portion of the myelinated axons (internodes) and the extracellular space surrounding the nodes of Ranvier (Salzer, 2003). A similar purpose, confinement of K^+ ions, would therefore be served at the vestibular calyceal synaptic cleft. Additionally many

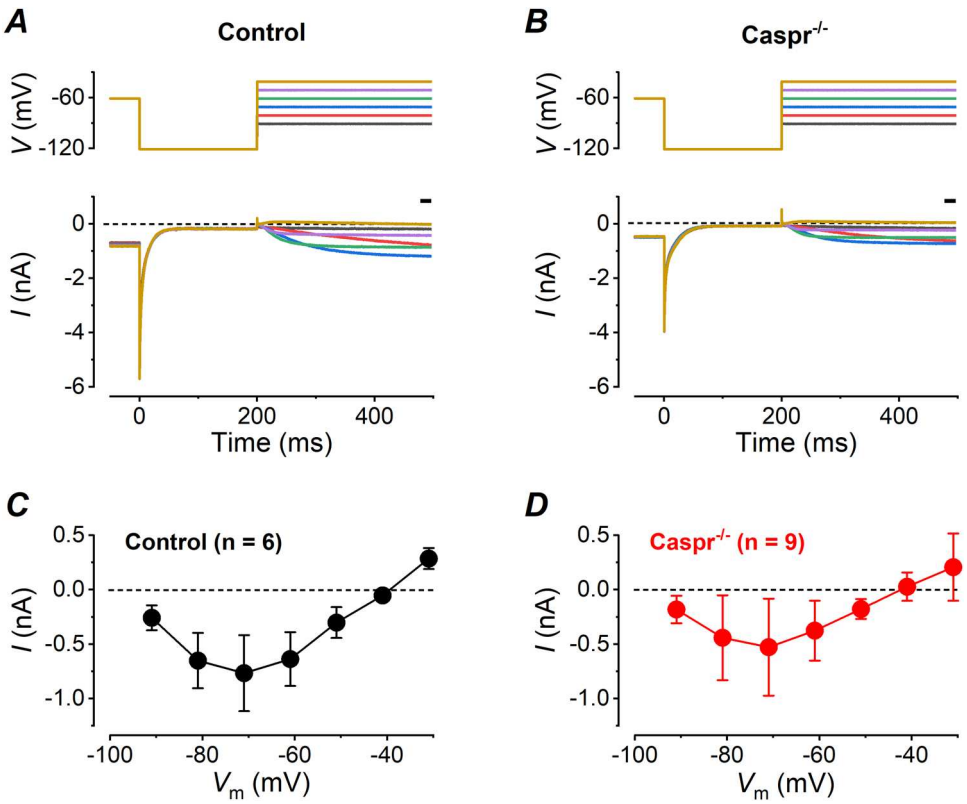

Figure 7. $G_{K,L}$ in control and *Caspr*$^{-/-}$ type I hair cells of mature mouse utricles
A, *B*, representative macroscopic currents from a type I hair cell of a control and a *Caspr*$^{-/-}$ mouse, respectively. Currents were recorded by using the CsGlutamate-based intracellular solution described in the Methods section. From a V_{hold} of −61 mV the cell was first hyperpolarized to −121 mV, and then iteratively depolarized by stepping the voltage from −91 to −31 mV in 10 mV increments, as shown by the voltage protocols shown in the upper panels. *C*, *D*, average steady-state macroscopic current measured in relation to the black bars shown above the traces as a function of V_m in control (n = 6) and *Caspr*$^{-/-}$ (n = 9) type I hair cells, respectively.

papers have shown that synaptic ectodomains and the proteins aggregated there also modulate the expression and function of nearby ion channels (Brockhaus et al., 2018; Wierda et al., 2020). For instance the septate junction protein Mesh plays an essential role in the physiological maturation and function of the Drosophila Malpighian tubule epithelium that is required for normal transepithelial fluid, ion transport and paracellular permeability (Jonusaite et al., 2020). Indeed Caspr is required for the recruitment or retention of KCNQ4 K^+ channels at the vestibular calyces (Sousa et al., 2009). However we found that the lack of Caspr did not affect the expression or properties of $G_{K,L}$. Therefore the smaller ΔC_m found in *Caspr*$^{-/-}$ type I hair cells is likely the consequence of the smaller R_c, given the larger distance between the hair cell basolateral membrane and the inner face of the calyx terminal compared with its wild-type counterpart (Sousa et al., 2009). However it cannot be excluded that this smaller ΔC_m could also be produced by the lack of the septate junction and/or by the proteins aggregated there, which could be not expressed, washed away or misplaced in the lack of this junction. These proteins could be charged and dragged in some way by the $G_{K,L}$ gate, amplifying the gating transient when they are present: on the basis of the literature cited above, these proteins could link pre- and post-synaptic elements, contributing to the accelerated synaptic transmission. It is excluded that the lack of these proteins decreases ΔC_m by slowing down the kinetics of the gating charge movement, and/or by decreasing the number of K,L channels, since this would affect the $I_{K,L}$ activation/deactivation kinetics and/or its amplitude, respectively, and this is not the case (Fig. 7).

As a final consideration, it is worth considering that R_c can only be estimated; that is, it cannot be measured directly. Recently, Cohen et al. (2020) estimated a resistivity of the extracellular solution of about 550 Ω cm at the paranode, i.e., about five times larger than that typically estimated for the resistivity of the extracellular solution at the calyceal synaptic cleft (100 Ω cm) (Govindaraju et al., 2023). Given its resemblance to the paranodal septate junction, even the resistivity of the extracellular solution at the calyceal synaptic cleft might be significantly higher than assumed, and so would R_c.

Indeed, despite piercing the calyx, recordings from the enclosed type I hair cell show that an outward K^+ current through $G_{K,L}$ of a few nA increased K^+ in the (residual) calyceal synaptic cleft of a few tens of mM (Contini et al., 2012; Spaiardi et al., 2017), as also shown by the following simple calculation. A $G_{K,L}$ current of amplitude i_K corresponds to an increase in the cleft concentration of n moles/s given by:

$$n = \frac{i_K}{eN_oC_v}$$

where e is the elementary charge, N_o is the Avogadro number and Vol_{cl} is the volume of the cleft (Table 1), which is

$$Vol_{cl} = \frac{4}{3}\,\pi\left[(r_h + s_c)^3 - {r_h}^3\right] f \approx 4\pi\, {r_h}^2 s_c f$$

In the Vol_{cl} expression the terms in ${s_c}^2$ and ${s_c}^3$ have been neglected because they are negligible in respect to ${r_h}^2$. Therefore:

$$n = \frac{i_K}{4\pi\, eN_o {r_h}^2 s_c f}$$

In round numbers, an i_K of ≈400 pA causes the cleft K^+ concentration to rise at a rate of $n = 3500$ mM/s in the absence of any transport (pumps, channels or exchangers) in the hair cell or in the calyx plasma membrane that removes cleft K^+. Assuming that the latter transports are not simultaneously activated to the i_K onset, the resting cleft K^+ concentration, $[K^+]_o \approx 5$ mM, would rise to an amount of $\Delta[K^+]_o \approx 4$ mM within 1 ms, causing a calyx depolarization of $\Delta V \approx 15$ mV due to its open K^+-permeable channels (mainly K_v7 ones) (Spitzmaul et al., 2013), according to:

$$\Delta V = \frac{RT}{F}\, ln\left(\frac{\left[K^+\right]_o + \Delta\left[K^+\right]_o}{\left[K^+\right]_o}\right)$$

that is enough to trigger an action potential in the calyx. This large K^+ efflux is not expected to cause any charge accumulation in the cleft, because of the rapid redistribution due to the strong electrostatic interaction between K^+ and the other ions (mainly Na^+ and Cl^-) present there. This calculation, although very basic, is in agreement with a very sophisticated model of the non-quantal transmission between type I hair cell and the calyx (Govindaraju et al., 2023), describing the kinetics of K^+ accumulation in the cleft.

Thus it seems reasonable to assume that, with an undamaged calyx, the resistivity of the extracellular solution in the synaptic cleft is higher than generally assumed, consistent with a residual R_c of about 40 MΩ in a pierced calyx (resulting from a ∼ 15 mV depolarization for an IK,L of ∼ 400 pA).

References

Armstrong, C. M. (1981). Sodium channels and gating currents. *Physiological Reviews*, **61**(3), 644–683.

Augustine, G. J., Santamaria, F., & Tanaka, K. (2003). Local calcium signaling in neurons. *Neuron*, **40**(2), 331–346.

Banerjee, S., Sousa, A. D., & Bhat, M. A. (2006). Organization and function of septate junctions: An evolutionary perspective. *Cell Biochemistry and Biophysics*, **46**(1), 65–77.

Barnett, D. W., & Misler, S. (1997). An optimized approach to membrane capacitance estimation using dual-frequency excitation. *Biophysical Journal*, **72**(4), 1641–1658.

Bonsacquet, J., Brugeaud, A., Compan, V., Desmadryl, G., & Chabbert, C. (2006). AMPA type glutamate receptor mediates neurotransmission at turtle vestibular calyx synapse. *The Journal of Physiology*, **576**(Pt 1), 63–71.

Brockhaus, J., Schreitmuller, M., Repetto, D., Klatt, O., Reissner, C., Elmslie, K., Heine, M., & Missler, M. (2018). α-Neurexins together with $\alpha 2\delta$-1 auxiliary subunits regulate $Ca(2^+)$ influx through Cav2.1 channels. *Journal of Neuroscience*, **38**, 8277–8294.

Burns, J. C., On, D., Baker, W., Collado, M. S., & Corwin, J. T. (2012). Over half the hair cells in the mouse utricle first appear after birth, with significant numbers originating from early postnatal mitotic production in peripheral and striolar growth zones. *Journal of the Association for Research in Otolaryngology*, **13**(5), 609–627.

Burns, J. C., & Stone, J. S. (2017). Development and regeneration of vestibular hair cells in mammals. *Seminars in Cell & Developmental Biology*, **65**, 96–105.

Catacuzzeno, L., Conti, F., & Franciolini, F. (2023). Fifty years of gating currents and channel gating. *Journal of General Physiology*, **155**(8), e202313380.

Chen, J. W., & Eatock, R. A. (2000). Major potassium conductance in type I hair cells from rat semicircular canals: Characterization and modulation by nitric oxide. *Journal of Neurophysiology*, **84**(1), 139–151.

Cohen, C. C. H., Popovic, M. A., Klooster, J., Weil, M. T., Möbius, W., Nave, K. A., & Kole, M. H. P. (2020). Saltatory conduction along myelinated axons involves a periaxonal nanocircuit. *Cell*, **180**(2), 311–322.e15.

Contini, D., Zampini, V., Tavazzani, E., Magistretti, J., Russo, G., Prigioni, I., & Masetto, S. (2012). Intercellular K^+ accumulation depolarizes type I vestibular hair cells and their associated afferent nerve calyx. *Neuroscience*, **227**, 232–246.

Contini, D., Price, S. D., & Art, J. J. (2017). Accumulation of K^+ in the synaptic cleft modulates activity by influencing both vestibular hair cell and calyx afferent in the turtle. *The Journal of Physiology*, **595**(3), 777–803.

Contini, D., Holstein, G. R., & Art, J. J. (2022). Simultaneous dual recordings from vestibular hair cells and their calyx afferents demonstrate multiple modes of transmission at these specialized endings. *Frontiers in Neurology*, **13**, 891536.

Contini, D., Holstein, G. R., & Art, J. J. (2024). Simultaneous recordings from vestibular type I hair cells and their calyceal afferents in mice. *Frontiers in Neurology*, **15**, 1434026.

Correia, M. J., & Lang, D. G. (1990). An electrophysiological comparison of solitary type I and type II vestibular hair cells. *Neuroscience Letters*, **116**, 106–111.

Dulon, D., Safieddine, S., Jones, S. M., & Petit, C. (2009). Otoferlin is critical for a highly sensitive and linear calcium-dependent exocytosis at vestibular hair cell ribbon synapses. *Journal of Neuroscience*, **29**(34), 10474-10487.

Gilly, W. F., & Armstrong, C. M. (1980). Gating current and potassium channels in the giant axon of the squid. *Biophysical Journal*, **29**(3), 485–492.

Goldberg, J. M. (1996). Theoretical analysis of intercellular communication between the vestibular type I hair cell and its calyx ending. *Journal of Neurophysiology*, **76**(3), 1942–1957.

Gollan, L., Salomon, D., Salzer, J. L., & Peles, E. (2003). Caspr regulates the processing of contactin and inhibits its binding to neurofascin. *The Journal of Cell Biology*, **163**(6), 1213–1218.

Govindaraju, A. C., Quraishi, I. H., Lysakowski, A., Eatock, R. A., & Raphael, R. M. (2023). Nonquantal transmission at the vestibular hair cell-calyx synapse: KLV currents modulate fast electrical and slow K^+ potentials. *Proceedings National Academy of Science USA*, **120**(2), e2207466120.

Holt, J. C., Chatlani, S., Lysakowski, A., & Goldberg, J. M. (2007). Quantal and nonquantal transmission in calyx-bearing fibers of the turtle posterior crista. *Journal of Neurophysiology*, **98**(3), 1083–1101.

Horrigan, F. T., & Bookman, R. J. (1994). Releasable pools and the kinetics of exocytosis in adrenal chromaffin cells. *Neuron*, **13**(5), 1119–1129.

Huang, S., Chen, J., Song, M., Yu, Y., Geng, J., Lin, D., Yang, J., Wu, J., Li, K., Yu, Y., Wang, J., Hu, L., Shan, Q., Wang, J., Chen, P., & Chen, F. (2023). Whole-exome sequencing and electrophysiological study reveal a novel loss-of-function mutation of KCNA10 in epinephrine provoked long QT syndrome with familial history of sudden cardiac death. *Legal Medicine (Tokyo, Japan)*, **62**, 102245.

Hurley, K. M., Gaboyard, S., Zhong, M., Price, S. D., Wooltorton, J. R., Lysakowski, A., & Eatock, R. A. (2006). M-like K^+ currents in type I hair cells and calyx afferent endings of the developing rat utricle. *Journal of Neuroscience*, **26**(40), 10253–10269.

Johnson, S. L., Thomas, M. V., & Kros, C. J. (2002). Membrane capacitance measurement using patch clamp with integrated self-balancing lock-in amplifier. *Pflugers Archiv: European Journal of Physiology*, **443**(4), 653–663.

Johnson, S. L., Marcotti, W., & Kros, C. J. (2005). Increase in efficiency and reduction in $Ca2^+$ dependence of exocytosis during development of mouse inner hair cells. *The Journal of Physiology*, **563**(Pt 1), 177–191.

Jonusaite, S., Beyenbach, K. W., Meyer, H., Paululat, A., Izumi, Y., Furuse, M., & Rodan, A. R. (2020). The septate junction protein Mesh is required for epithelial morphogenesis, ion transport, and paracellular permeability in the Drosophila Malpighian tubule. *American Journal of Physiology-Cell Physiology*, **318**(3), C675–C694.

Kilic, G., & Lindau, M. (2001). Voltage-dependent membrane capacitance in rat pituitary nerve terminals due to gating currents. *Biophysical Journal*, **80**(3), 1220–1229.

Lim, R., Kindig, A. E., Donne, S. W., Callister, R. J., & Brichta, A. M. (2011). Potassium accumulation between type I hair cells and calyx terminals in mouse crista. *Experimental Brain Research*, **210**(3–4), 607–621.

Lu, C. C., Kabakov, A., Markin, V. S., Mager, S., Frazier, G. A., & Hilgemann, D. W. (1995). Membrane transport mechanisms probed by capacitance measurements with megahertz voltage clamp. *Proceedings of the National Academy of Sciences of the United States of America*, **92**(24), 11220–11224.

Lysakowski, A., & Goldberg, J. M. (2004). Morphophysiology of the vestibular periphery. In: *The Vestibular System*, pp 57–152. Springer Hearing and Auditory Research. Springer New York.

Manca, M., Yen, P., Spaiardi, P., Russo, G., Giunta, R., Johnson, S. L., Marcotti, W., & Masetto, S. (2021). Current response in Ca V 1.3-/- mouse vestibular and cochlear hair cells. *Frontiers in Neuroscience*, **15**, 749483.

Martin, H. R., Lysakowski, A., & Eatock, R. A. (2024). The potassium channel subunit KV1.8 (Kcna10) is essential for the distinctive outwardly rectifying conductances of type I and II vestibular hair cells. *eLife*, **13**, RP94342.

Matsubara, A., Takumi, Y., Nakagawa, T., Usami, S., Shinkawa, H., & Ottersen, O. P. (1999). Immunoelectron microscopy of AMPA receptor subunits reveals three types of putative glutamatergic synapse in the rat vestibular end organs. *Brain Research*, **819**(1–2), 58–64.

Matthews, G., & Fuchs, P. (2010). The diverse roles of ribbon synapses in sensory neurotransmission. *Nature Reviews Neuroscience*, **11**(12), 812–822.

Michanski, S., Henneck, T., Mukhopadhyay, M., Steyer, A. M., Gonzalez, P. A., Grewe, K., Ilgen, P., Gültas, M., Fornasiero, E. F., Jakobs, S., Möbius, W., Vogl, C., Pangršič, T., Rizzoli, S. O., & Wichmann, C. (2023). Age-dependent structural reorganization of utricular ribbon synapses. *Frontiers in Cell and Developmental Biology*, **11**, 1178992.

Mukhopadhyay, M., & Pangrsic, T. (2022). Synaptic transmission at the vestibular hair cells of amniotes. *Molecular and Cellular Neuroscience*, **121**, 103749.

Neher, E. (1998). Vesicle pools and Ca^{2+} microdomains: New tools for understanding their roles in neurotransmitter release. *Neuron*, **20**(3), 389–399.

Pangrsic, T., Singer, J. H., & Koschak, A. (2018). Voltage-gated calcium channels: Key players in sensory coding in the retina and the inner ear. *Physiological Reviews*, **98**(4), 2063–2096.

Rennie, K. J., & Correia, M. J. (1994). Potassium currents in mammalian and avian isolated type I semicircular canal hair cells. *Journal of Neurophysiology*, **71**(1), 317–329.

Rennie, K. J., & Correia, M. J. (2000). Effects of cationic substitutions on delayed rectifier current in type I vestibular hair cells. *Journal of Membrane Biology*, **173**(2), 139–148.

Rüsch, A., & Eatock, R. A. (1996). A delayed rectifier conductance in type I hair cells of the mouse utricle. *Journal of Neurophysiology*, **76**(2), 995–1004.

Sadeghi, S. G., Pyott, S. J., Yu, Z., & Glowatzki, E. (2014). Glutamatergic signaling at the vestibular hair cell calyx synapse. *Journal of Neuroscience*, **34**(44), 14536–14550.

Salzer, J. L. (2003). Polarized domains of myelinated axons. *Neuron*, **40**(2), 297–318.

Santos-Sacchi, J. (2004). Determination of cell capacitance using the exact empirical solution of partial differential Y/partial differential Cm and its phase angle. *Biophysical Journal*, **87**(1), 714–727.

Singer, J. H., & Diamond, J. S. (2003). Sustained Ca^{2+} entry elicits transient postsynaptic currents at a retinal ribbon synapse. *Journal of Neuroscience*, **23**(34), 10923–10933.

Songer, J. E., & Eatock, R. A. (2013). Tuning and timing in mammalian type I hair cells and calyceal synapses. *Journal of Neuroscience*, **33**(8), 3706–3724.

Sousa, A. D., Andrade, L. R., Salles, F. T., Pillai, A. M., Buttermore, E. D., Bhat, M. A., & Kachar, B. (2009). The septate junction protein caspr is required for structural support and retention of KCNQ4 at calyceal synapses of vestibular hair cells. *Journal of Neuroscience*, **29**(10), 3103–3108.

Spaiardi, P., Tavazzani, E., Manca, M., Milesi, V., Russo, G., Prigioni, I., Marcotti, W., Magistretti, J., & Masetto, S. (2017). An allosteric gating model recapitulates the biophysical properties of IK, L expressed in mouse vestibular type I hair cells. *The Journal of Physiology*, **595**, 6735–6750.

Spaiardi, P., Marcotti, W., Masetto, S., & Johnson, S. L. (2020). Exocytosis in mouse vestibular type II hair cells shows a high-order Ca^{2+} dependence that is independent of synaptotagmin-4. *Physiological Reports*, **8**(14), e14509.

Spaiardi, P., Tavazzani, E., Manca, M., Russo, G., Prigioni, I., Biella, G., Giunta, R., Johnson, S. L., Marcotti, W., & Masetto, S. (2020). K^+ accumulation and clearance in the calyx synaptic cleft of type I mouse vestibular hair cells. *Neuroscience*, **426**, 69–86.

Spaiardi, P., Marcotti, W., Masetto, S., & Johnson, S. L. (2022). Signal transmission in mature mammalian vestibular hair cells. *Frontiers in Cellular Neuroscience*, **16**, 806913.

Spitzmaul, G., Tolosa, L., Winkelman, B. H., Heidenreich, M., Frens, M. A., Chabbert, C., de Zeeuw, C. I., & Jentsch, T. J. (2013). Vestibular role of KCNQ4 and KCNQ5 K+ channels revealed by mouse models. *Journal of Biological Chemistry*, **288**(13), 9334–9344.

Vincent, P., Bouleau, Y., Safieddine, S., Petit, C., & Dulon, D. (2014). Exocytotic machineries of vestibular type I and cochlear ribbon synapses display similar intrinsic otoferlin-dependent Ca^{2+} sensitivity but a different coupling to $Ca2^{+}$ channels. *Journal of Neuroscience*, **34**, 10853–10869.

Wersäll, J. (1956). Studies on the structure and innervation of the sensory epithelium of the cristae ampulares in the guinea pig; a light and electron microscopic investigation. *Acta Oto-Laryngologica Supplementum*, **126**, 1–85.

Wierda, K. D. B., Toft-Bertelsen, T. L., & Gøtzsche, C. R., Pedersen, E., Korshunova, I., Nielsen, J., Bang, M. L., Kønig, A. B., Owczarek, S., Gjørlund, M. D., Schupp, M., Bock, E., & Sørensen, J. B. (2020). The soluble neurexin-1β ectodomain causes calcium influx and augments dendritic outgrowth and synaptic transmission. *Scientific Reports*, **10**, 18041.

Yamashita, M., & Ohmori, H. (1990). Synaptic responses to mechanical stimulation in calyceal and bouton type vestibular afferents studied in an isolated preparation of semicircular canal ampullae of chicken. *Experimental Brain Research*, **80**(3), 475–488.

Yamashita, T., Eguchi, K., Saitoh, N., von Gersdorff, H., & Takahashi, T. (2010). Developmental shift to a mechanism of synaptic vesicle endocytosis requiring nanodomain Ca^{2+}. *Nature Neuroscience*, **13**(7), 838–844.

Additional information

Data availability statement

Data will be made available upon reasonable request.

Competing interests

The authors declare that they have no competing interests.

Author contributions

P.S., S.M. and S.L.J. designed the study. P.S. and S.L.J. performed the experiments. P.S., S.M., G.R. and S.L.J. analysed and interpreted the data. P.S., S.M., G.R., R.G. and S.L.J. critically revised and approved the final version of the manuscript submitted for publication.

Funding

This work was supported by grants from THE EUROPEAN UNION – NEXT GENERATION EU, PNRR M4.C2.1.1 – 20228AAJRL – Signal transmission at the mammalian vestibular hair cell synapses – CUP: F53D23005930006 to Sergio Masetto and Giorgio Rispoli. THE EUROPEAN UNION – NEXT GENERATION EU, Missione 4 Componente 1 – 2022KNFAYR—BIO-SMILE: BIOmedical restoration of Symmetrical Motor control in unilateral paraLysEs due to nerve lesions – CUP: F53D23006030001. BBSRC (BB/X000567/1) and RNID (G106) to Stuart L Johnson.

Acknowledgements

Caspr mice were a kind gift from Prof. Elior Peles, Weitzmann Institute of Science (Rehovot, Israel).

Open access publishing facilitated by Universita di Pavia, as part of the Wiley - CRUI-CARE agreement.

Keywords

cell membrane capacitance, exocytosis, gating current, hair cell, vestibular

Supporting information

Additional supporting information can be found online in the Supporting Information section at the end of the HTML view of the article. Supporting information files available:

Peer Review History